Since January 2020 Elsevier has created a COVID-19 resource centre with free information in English and Mandarin on the novel coronavirus COVID-19. The COVID-19 resource centre is hosted on Elsevier Connect, the company's public news and information website.

Available online at www.sciencedirect.com
ScienceDirect
Biochimica et Biophysica Acta 1774 (2007) 1237–1246
Biochimica et Biophysica Acta
BBA
www.elsevier.com/locate/bbapap

Proteomic analysis of cathepsin B and L-deficient mouse brain lysosomes

Sonja Stahl [a], Yvonne Reinders [b], Esther Asan [c], Walther Mothes [d], Ernst Conzelmann [e], Albert Sickmann [b], Ute Felbor [a,*]

[a] Department of Human Genetics, University of Würzburg, Biozentrum, Am Hubland, D-97074 Würzburg, Germany
[b] Rudolf-Virchow-Center for Experimental Biomedicine, University of Würzburg, Germany
[c] Department of Anatomy and Cell Biology, University of Würzburg, Germany
[d] Section of Microbial Pathogenesis, Yale University School of Medicine, New Haven, CT, USA
[e] Department of Physiological Chemistry II, University of Würzburg, Germany

Received 18 February 2007; received in revised form 25 May 2007; accepted 6 July 2007
Available online 19 July 2007

Abstract

Cathepsins B and L are lysosomal cysteine proteases which have been implicated in a variety of pathological processes such as cancer, tumor angiogenesis, and neurodegeneration. However, only a few protein substrates have thus far been described and the mechanisms by which cathepsins B and L regulate cell proliferation, invasion, and apoptosis are poorly understood. Combined deficiency of both cathepsins results in early-onset neurodegeneration in mice reminiscent of neuronal ceroid lipofuscinoses in humans. Therefore, we intended to quantify accumulated proteins in brain lysosomes of double deficient mice. A combination of subcellular fractionation and LC-MS/MS using isobaric tagging for relative and absolute quantitation (iTRAQ™) allowed us to simultaneously assess wildtype and cathepsin $B^{-/-}L^{-/-}$ cerebral lysosomes. Altogether, 19 different proteins were significantly increased in cathepsin $B^{-/-}L^{-/-}$ lysosomes. Most elevated proteins had previously been localized to neuronal biosynthetic, recycling/endocytic or lysosomal compartments. A more than 10-fold increase was observed for Rab14, the Delta/Notch-like epidermal growth factor-related receptor (DNER), calcyon, and carboxypeptidase E. Intriguingly, immunohistochemistry demonstrated that Rab14 and DNER specifically stain swollen axons in double deficient brains. Since dense accumulations of expanded axons are the earliest phenotypic and pathognomonic feature of cathepsin $B^{-/-}L^{-/-}$ brains, our data suggest a role for cathepsins B and L in recycling processes during axon outgrowth and synapse formation in the developing postnatal central nervous system.

Keywords: Cerebrum; Cathepsin B; Cathepsin L; Lysosome; iTRAQ™; LC-MS/MS

1. Introduction

Cathepsins B and L belong to a family of 11 cysteine proteases (cathepsins B, C, H, F, K, L, O, S, V, W, and X/Z) with major roles in terminal protein degradation within the lysosome. Specific protein processing functions in other cellular compartments have more recently been recognized for the widely expressed cathepsins B and L. These include regulation of cell cycle progression through proteolytic processing of the CDP/Cux transcription factor in the nucleus [1], major histocompatibility complex class II antigen presentation [2] and control of growth factor recycling in endosomes [3], and hormone production within the regulated secretory pathway [4–6]. Notably, cathepsin L has been shown to convert proenkephalin to the active enkephalin opioid peptide neurotransmitter within secretory vesicles of neuroendocrine chromaffin cells [5]. Cathepsin B has been proposed to act as a β-secretase producing neurotoxic Aβ [7]. However, it was just shown that cathepsin B also degrades preformed extracellular oligomeric and fibrillar amyloid in aged APP transgenic mice [8]. Furthermore, cathepsin B was identified as the major enzyme responsible for endosomal proteolysis of internalized epidermal growth factor receptor complexes [9] and insulin-like growth factor-I [10]. Multistep endosomal proteolysis involving cathepsins B and L is also required for Ebola virus [11] and SARS-coronavirus infection [12].

During certain pathological conditions such as tumor invasion and tumor angiogenesis, both cathepsins have been reported to be upregulated, translocated to the cell surface, and secreted. Secreted procathepsin L generates the angiogenesis inhibitor

* Corresponding author. Tel.: +49 931 888 4097; fax: +49 931 888 4058.
E-mail address: felbor@biozentrum.uni-wuerzburg.de (U. Felbor).

1570-9639/$ - see front matter © 2007 Elsevier B.V. All rights reserved.
doi:10.1016/j.bbapap.2007.07.004

endostatin from collagen XVIII after conversion to mature cathepsin L in the acidic extracellular milieu of murine hemangioendothelioma cells [13]. In a mouse model of pancreatic islet cell carcinogenesis, impaired tumor invasion in cathepsin $B^{-/-}$ mice and cathepsin $L^{-/-}$ mice was in part attributed to maintenance of E-cadherin protein levels. It was subsequently demonstrated that both cathepsins release the extracellular domain of E-cadherin *in vitro* which abrogates its adhesive function [14]. Both single knockout mice also showed a reduction of tumor cell proliferation and increased cell death. The latter could be correlated with observed defects in tumor angiogenesis only in cathepsin $B^{-/-}$ mice. Thus, apoptosis occurred independently of angiogenesis defects in cathepsin $L^{-/-}$ mice [14].

The role of cathepsins in apoptosis appears to be complex. Cathepsin B has been reported to be an essential downstream mediator during tumor cell apoptosis induced by tumor necrosis factor (TNF-α) [15]. This lysosomal pathway of apoptosis requires the release of lysosomal enzymes into the cytoplasm (reviewed in [16]) and can be inhibited by suppression of cytosolic cathepsin B activity [17]. Furthermore, increased proteolysis by cathepsin B contributes to neuronal apoptosis in cystatin B-deficient mice, a murine model of Unverricht–Lundborg progressive myoclonus epilepsy [18]. However, the biological relevance of the reported *in vitro* cleavage of the proapoptotic BCl-2 family member Bid by cathepsins [19] has been questioned *in vivo* [20], and further cytosolic target proteins of cathepsin B are not known. In contrast to the observed increased resistance of cathepsin $B^{-/-}$ cells to TNF-α-triggered apoptosis [15], cathepsin L-deficient lung carcinoma cells showed increased sensitivity to apoptosis [21] which is in agreement with increased tumor cell death in the mouse model of multistage pancreatic tumorigenesis after deletion of cathepsin L [14]. Increased apoptosis in the absence of cathepsin L could be rescued by inhibition of the aspartic protease cathepsin D whose single-chain isoform was subsequently shown to be specifically degraded by cathepsin L. Therefore, it was proposed that cathepsin L contributes to control death receptor-induced apoptosis via proteolysis of cathepsin D [21].

Cathepsin $B^{-/-}L^{-/-}$ mice display a pronounced lysosomal storage disease leading to extensive neuron death in the central nervous system and develop a pronounced brain atrophy during the fourth postnatal week (Table 1) [22]. Most double mutant animals die during the weaning period even if they are carefully nursed. Procathepsin D and correctly processed mature cathepsin D were found to be increased in cathepsin $B^{-/-}L^{-/-}$ brain lysates [22] which potentially adds to the terminal apoptotic process. However, prior to neuronal cell death, cathepsin $B^{-/-}L^{-/-}$ neurons develop a lysosomal storage disorder reminiscent of human neuronal ceroid lipofuscinoses [22,23]. This suggests that cathepsins B and L have other essential roles during postnatal maturation and in maintaining the integrity of the central nervous system. In addition, cathepsin D deficiency or dysfunction itself causes a congenital form of neuronal ceroid lipofuscinoses in mice [24], sheep [25] and humans [26,27].

Cathepsins B and L can compensate for each other *in vivo* since only cathepsin $B^{-/-}L^{-/-}$ double mutant mice and not the respective single knockout mice develop autophagosomal and lysosomal accumulations within neurons. Importantly, the phenotype is restricted to select neurons in the cerebral and cerebellar cortex. In order to identify common neuronal substrates of cathepsins B and L, we performed a subcellular proteomics approach combining subcellular fractionation and amine-specific isobaric tag-based protein quantification by LC-MS/MS. Here, we present 19 proteins which are significantly increased in cathepsin $B^{-/-}L^{-/-}$ brain lysosomes. Our results imply that cathepsins B and L are involved in biosynthetic and recycling processes during early postnatal brain development.

Table 1
Summary of histologically detectable phenotypic features of cathepsin $B^{-/-}L^{-/-}$ mice complemented with biochemical data [22]

Age in days	Phenotype
P0.5	Swollen axons in white matter
P3.5	Dense accumulation of swollen axons in axon-rich areas
P3.5	Broadened hippocampal stratum pyramidale
P10.5	Klüver–Barrera-positive inclusions in cerebral neurons
P12.5	Normal PPT activity in $B^{-/-}L^{-/-}$ brain lysates
P17.5	Increased PPT activity in $B^{-/-}L^{-/-}$ brain lysates
P17.5	Apoptosis of cerebellar Purkinje cells
P21.5	Apoptosis of select neurons in the cerebral cortex

P=postnatal, PPT=Palmitoyl-protein thioesterase 1.

2. Experimental procedures

2.1. Mice

Cathepsin $B^{-/-}L^{-/-}$ mice were described previously [13]. Both double mutant and wild-type controls were from a mixed genetic background (C57BL/6×129/sv). All animal experiments were performed in compliance with institutional guidelines.

2.2. Subcellular fractionation

P17.5 double mutant and control cerebral tissues were dissected after intracardiac perfusion with cold 140 mM NaCl, 10 mM Tris–HCl, pH 7.4, in order to minimize red blood cell content. All following steps were performed at 4 °C. Perfused mouse brains were immediately homogenized in an isoosmotic homogenization buffer (0.25 M sucrose containing 1 mM EDTA, 100 μM leupeptin, 100 μM elastinatinal, 50 μM pepstatinA) by five passes with 1000 U/min using a Potter S homogenizer (Braun). After a centrifugation step of 1000 rpm for 2 min, 2 ml postnuclear supernatants were loaded onto 10 ml 41% Percoll (Amersham Pharmacia Biotech) in 0.25 M sucrose which had been layered on top of a 1-ml cushion of 90% Percoll. After 30 min centrifugation at 25,000 rpm and 4 °C (Beckman L8-70M), 500 μl subcellular fractions were collected from the bottom of the tube.

2.3. Biochemical characterization of subcellular fractions

10 μl of each fraction were mixed with 90 μl 0.25% Triton X-100 to disrupt lysosomes and the specific hexosaminidase substrate 4-methylumbelliferyl-β-D-N-acetylglucosaminide (Sigma) was added. After 30 min of incubation at 37 °C, the amount of the fluorescent product 4-methylumbelliferone was detected with a fluorimeter at 440 nm after excitation at 366 nm. Further enzymatic activities analyzed were 2′,3′-phosphodiesterase for myelin, catalase for peroxisomes, succinate-dehydrogenase for mitochondria, and cholin acetyl transferase for synaptosomes using the substrates adenosine 2′3′-cyclic monophosphate (Sigma), hydrogen peroxide, natrium succinate (Sigma), and [1-^{14}C]acetyl CoA, respectively.

10 μl of all wild-type and double knockout fractions were also loaded onto 10–20% SDS-PAGE gels, electroblotted onto nitrocellulose and probed with a polyclonal rat anti-mouse LAMP-1 antibody (PharMingen, 553792). Further

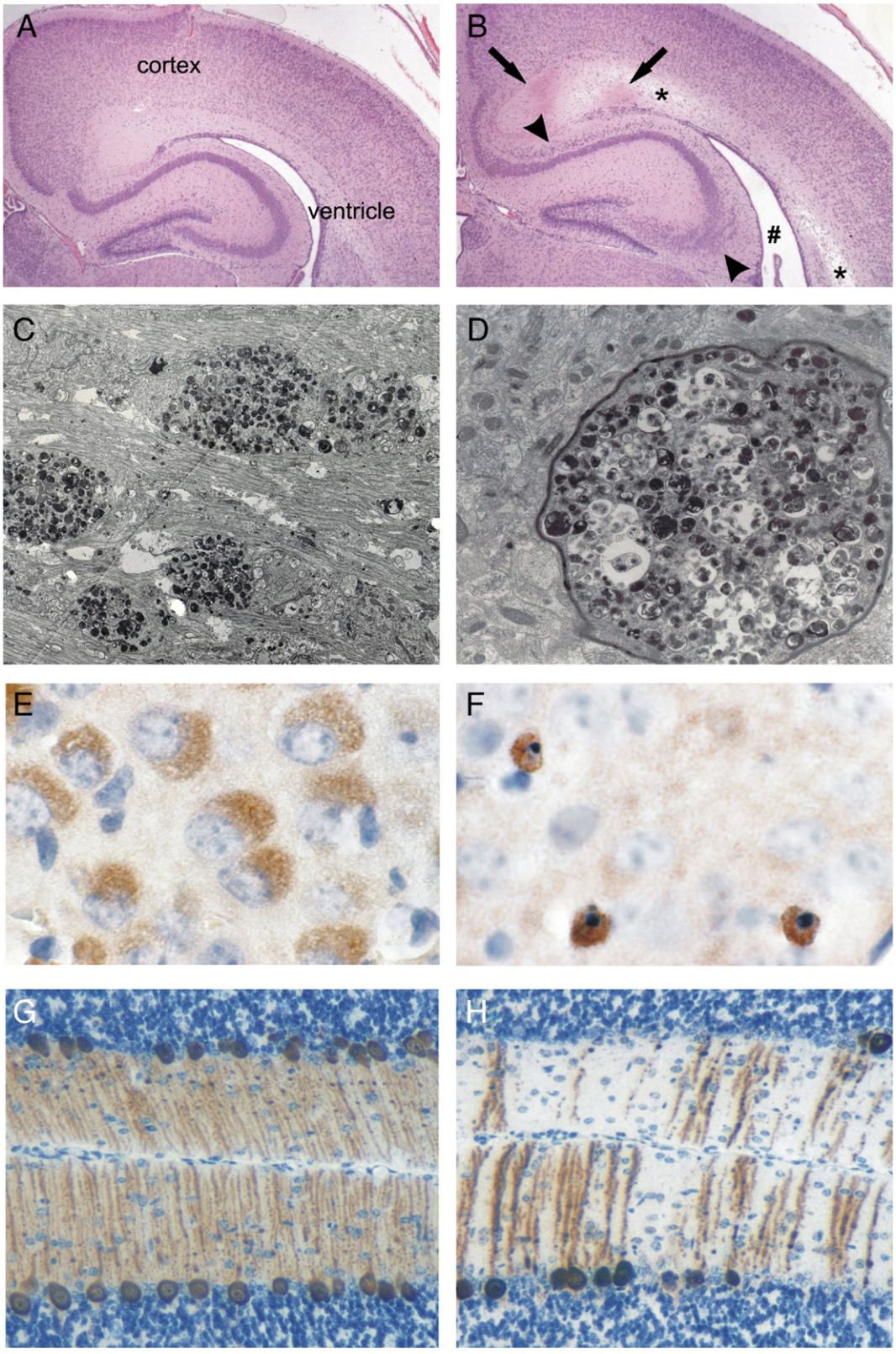

Fig. 1. The cathepsin $B^{-/-}/L^{-/-}$ phenotypes. (A) P5.5 wild type and (B) double knockout mouse section demonstrating areas of densely packed, expanded axons in the $B^{-/-}/L^{-/-}$ corpus callosum (arrows, higher magnifications can be seen in [22]), broadening of the hippocampal stratum pyramidale (arrow heads), white matter hypodensity (*), and enlarged ventricles (#). (C) Electron micrograph of swollen axons in the corpus callosum of a P24.5 $B^{-/-}/L^{-/-}$ mouse. (D) Multivesicular axonal inclusions in the optic nerve of a $B^{-/-}/L^{-/-}$ mouse nursed for 90 days. (E) P17.5 double mutant neuronal perikarya in the cerebral cortex are ballooned due to lysosomal storage and react with an antibody against activated caspase-3. (F) Apoptotic caspase-3-positive neurons in the cerebrum at P24.5. (G) P17.5 wild type cerebellar Purkinje cells (brown) labeled with an antibody against calbindin. (H) P17.5 $B^{-/-}/L^{-/-}$ Purkinje cells disappear during that stage.

antibodies were a mouse anti-rat neuronal class III β-tubulin (TUJ1) antibody (Convance, MMS-435P), a goat anti-human cathepsin D antibody (Santa Cruz Biotechnology, sc-6486), a rabbit anti-human Rab14 antibody (abcam, ab28639), a goat anti-mouse DNER antibody (R&D Systems, AF2254). Secondary antibodies conjugated to peroxidase were purchased from Dianova.

2.4. Electron microscopy

To eliminate Percoll particles, pooled fractions 3–5 containing double knockout lysosomes were centrifuged at 100,000×*g* (4 °C). The white interphase was diluted with 0.25 M sucrose (60 μl) and fixed for 90 min with 2% glutaraldehyde in 0.1 M phosphate-buffered saline, pH 7.4, at 4 °C. A light yellow pellet became visible that was washed with PBS and spun at 40,000 rpm for 15 min at 4 °C three times. The pellet was then incubated in 1% OsO_4 in PBS for 1 h and washed three times for 15 min in ddH_2O. After dehydratation in graded ethanol, the pellet was epon-embedded. Ultrathin sections were contrasted with uranyl acetate and lead citrate according to standard protocols and examined with a transmission electron microscope (LEO 912 AB, Zeiss SMT, Oberkochen, Germany).

Electron microscopy of brains and the optic nerve was performed as described previously [22].

2.5. Isobaric tagging for relative and absolute quantitation (iTRAQ™ labeling)

Lysosomes derived from fractions 3 to 5 were resuspended in 20 μl digestion buffer (0.5 M triethylammonium bicarbonate, pH 8.5, and 0.1% SDS). The final protein concentration was determined with the bicinchoniic acid assay (Pierce). iTRAQ™ reagents were dissolved in 70 μl ethanol. 50 μg protein was reduced for 60 min at 37 °C using reducing reagent, blocked for 10 min at room temperature using MMTS, and digested with trypsin over night. Afterwards, each sample was incubated with a different iTRAQ™ reagent for 1 h.

2.6. Cation exchange chromatography

After pooling the samples, the mixture was separated directly by cation exchange chromatography as previously described [28]. Prior to nano-LC-MS/MS, each fraction was concentrated in a vacuum centrifuge to diminish the acetonitrile concentration.

2.7. Nano-rechromatography and MS/MS

The sample was preconcentrated on a C_{18} precolumn (C_{18} PepMap™ RP, 300 μm ID × 1 mm, Dionex, Idstein, Germany) for 5 min at a flow rate of 25 μl/min using an HPLC system consisting of a Famos™ autosampler, a Switchos™ microcolumn switching module and an Ultimate™ micropump (all Dionex). Afterwards, peptides were eluted and separated on a C_{18} main column (C_{18} PepMap™ RP, 75 μm ID × 150 mm, Dionex) by a binary gradient composed of solvent A (0.1% formic acid) and solvent B (0.1% formic acid in 84% acetonitrile). Solvent B was increased linearly from 5% to 50% within 30 min, then to 95% for 10 min, and afterwards the column was reequilibrated to 5% solvent B. The flow rate was set to 250 nL/min. Peptides were directly eluted into an ESI-mass spectrometer. For mass spectrometric analysis a Quad-TOF QStar®XL (Applied Biosystems, Darmstadt, Germany) was used.

2.8. Data analysis

Data analysis of the derived spectra was accomplished using the ProQUANT 1.0 software (Applied Biosystems, Darmstadt, Germany) for both identification and quantification. Database searching was restricted to tryptic peptides of the NCBI mouse protein database (June 2005). For iTRAQ™ experiments, side reactions with tyrosine were also taken into account. Doubly and triply charged ions were considered, respective mass tolerances were set to 0.2 Da. Proteins were identified on the basis of having at least one peptide whose individual ion score was above the 98% confidence threshold. The iTRAQ ratios reported are the average ratios calculated from the ratios of the individual peptides determined for each protein. All spectra were verified manually in order to avoid false positive hits derived from the search algorithms.

2.9. Histology and immunohistochemistry

Paraffin-embedded sections were stained with hematoxylin and eosin (H&E). Immunohistochemistry was performed on P15.5, P17.5 and P50.5 Bouins' fixed, paraffin-embedded brain sections with anti Rab14, DNER, cathepsin D (see above), activated caspase-3 (Cell Signaling Technology) and calbindin (Swant) antibodies using the Vectastain *Elite* ABC kit and the diaminobenzidene substrate kit from Vector Laboratories. Counterstaining was performed with hematoxylin or cresylecht violet.

3. Results

3.1. Isolation of lysosomes

The cathepsin B and L-deficient brain phenotype is complex and has been described in detail [22]. Densely packed swollen axons in white matter parts and a broadened hippocampus become apparent on postnatal day 3 (P3.5) (Fig. 1A, B; Table 1).

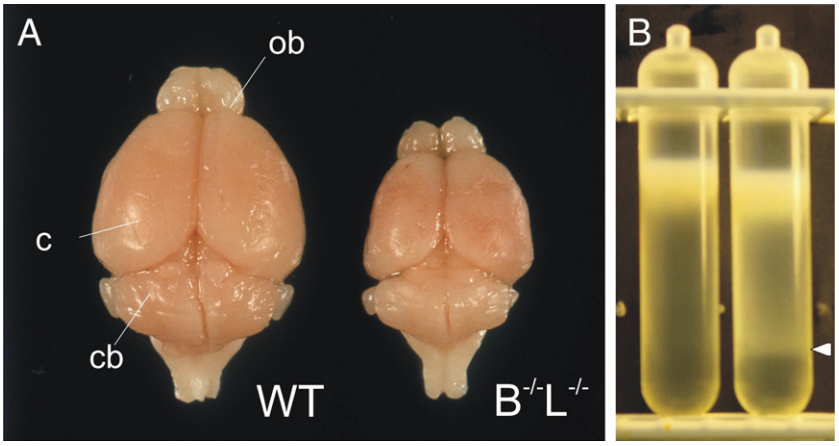

Fig. 2. Purification of cathepsin $B^{-/-}/L^{-/-}$ lysosomes from cerebral tissues. (A) 24-day-old wildtype (wt) and cathepsin $B^{-/-}/L^{-/-}$ mouse brains demonstrating a 35% reduction of the double mutant brain size mainly attributable to neuronal apoptosis [22]. The mean wet weight is 313 mg in controls and 203 mg in double mutant cerebra. In the present study, only the cerebrum (c) was analyzed (cb = cerebellum, ob = olfactory bulb). (B) Percoll gradients revealing a white band at the position of the heavy lysosomes (arrow) after centrifugation of cathepsin $B^{-/-}/L^{-/-}$ postnuclear supernatants (left: wild type; right: $B^{-/-}L^{-/-}$).

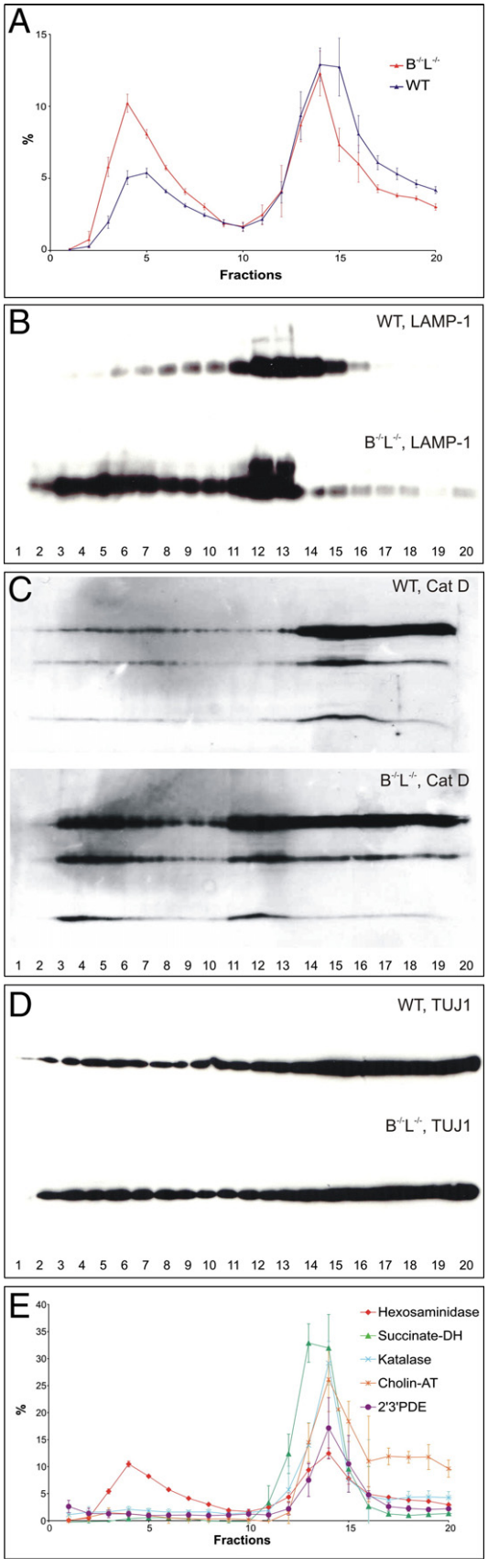

Fig. 3. Biochemical characterization of wildtype and cathepsin $B^{-/-}/L^{-/-}$ fractions. (A) Hexosaminidase assays of wildtype (green) and $B^{-/-}/L^{-/-}$ (red) fractions (average of five independent experiments). (B–D) fractions loaded onto 10–20% SDS-PAGE gels and probed with an antibody against LAMP1 (B), cathepsin D (C) and neuronal β-tubulin (D). (E) The lysosomal fractions 3–5 are clearly separated from mitochondria, synaptosomes, peroxisomes, and myelin in cathepsin $B^{-/-}/L^{-/-}$ lysosomes (average of five independent experiments). The enzymatic profiles of the respective wild-type fractions show no difference except for the hexosaminidase activities.

The expanded axons (Fig. 1C, D) contain a large number of dense bodies often filled with membraneous and vesicular material. On postnatal days 16 to 17 (P16.5–P17.5), perikarya of cathepsin $B^{-/-}/L^{-/-}$ cerebral neurons contain large amounts of lysosomal accumulations (Fig. 1E). Apoptotic cell death becomes prominent between P21.5 and P24.5 (Fig. 1F; Table 1). Since most double knockouts survive until P16.5–P17.5, this stage was chosen for further analyses. The cerebellum was excluded because apoptosis already peaks around day 17.5 in the Purkinje cell monolayer [22] (Fig. 1G, H; Table 1).

For resolution of lysosomal fractions, freshly perfused murine cerebral tissues (Fig. 2A) were homogenized. The postnuclear supernatants were subjected to density gradient subcellular fractionation. A 41% Percoll gradient allowed separation of a high-density (fractions 3–6) and a low-density peak (fractions 13–16) of β-hexosaminidase activity (Figs. 2B and 3A). Despite a significantly reduced mean wet weight of 203 mg for double mutants when compared to 313 mg for controls, a distinct white band became visible at the bottom of the double mutant gradient (Fig. 2B). Direct comparison of the distribution profile of β-hexosaminidase activity between wild-type and $B^{-/-}/L^{-/-}$ fractions revealed an obvious shift towards heavier lysosomes in $B^{-/-}/L^{-/-}$ brains (Fig. 3A). A similar difference in the profile of the endosomal–lysosomal compartment was observed upon SDS-PAGE and western blot analyses of all wild-type and double knockout fractions using an antibody against LAMP1 (Fig. 3B) and cathepsin D (Fig. 3C). Again, a prominent enrichment of late-stage lysosomes was found in double mutant mice. In contrast, the representative cytoskeletal marker TUJ1 only demonstrates a slight increase in heavy lysosomal fractions which may be explained by a general accumulation of proteins in cathepsin B and L-deficient lysosomes (Fig. 3D).

To assess the purity of the late-stage lysosomal fractions, all fractions were analyzed using enzymatic markers specific for mitochondria, synaptosomes, peroxisomes and myelin which proved to be absent in cathepsin $B^{-/-}/L^{-/-}$ lysosomal fractions 3–5 (Fig. 3E). Furthermore, electron microscopy demonstrated the high purity of intact, membrane-bound lysosomes containing electron-dense material in the pooled fractions 3–5 from double mutants (Fig. 4). Therefore, these fractions were chosen for further analyses.

3.2. Identification of proteins increased in cathepsin $B^{-/-}/L^{-/-}$ lysosomes

In order to compare the protein composition of cathepsin $B^{-/-}/L^{-/-}$ and wildtype lysosomes, a quantitative proteomic strategy using iTRAQ™ reagents and nano-LC-MS/MS was

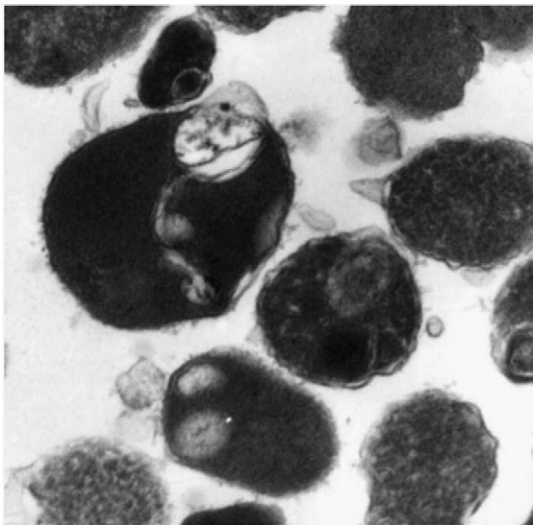

Fig. 4. Electron microscopy of purified cathepsin $B^{-/-}/L^{-/-}$ lysosomes. After subcellular fractionation, structurally intact, membrane-bound, electron-dense storage lysosomes were obtained which occasionally contain lamellae. Wild-type lysosomes which only rarely contain dense storage material were lost during preparation procedures.

employed. For protein quantification only peptides that had been identified by more than one, manually verified spectrum were considered. Furthermore, only proteins that were increased by at least a factor of four were taken into account. Thereby, a total of 19 unique murine proteins, summarized in Table 2, were found to be increased in cathepsin $B^{-/-}/L^{-/-}$ lysosomes. These include five lysosomal enzymes: acid ceramidase-like protein, cathepsin D, hexosaminidase A and B, and palmitoyl-protein thioesterase 1. In addition, the acidic glycoprotein prosaposine, a precursor of four activator proteins of various lysosomal enzymes was found to be increased. Two further proteins, ubiquitin B, and sequestosome 1, are part of ubiquitination-dependent degradation. Calcyon [29], apolipoprotein E [30,31], Rab14 [32], phospholipase D [33], carboxypeptidase E [34], and the Delta/Notch-like epidermal growth factor-related receptor (DNER) [35] have been found in secretory and recycling pathways. Thus, most of the proteins presented in Table 2 have been associated with biosynthetic, endocytic, and lysosomal compartments. Moreover, the majority of the proteins identified are known to be expressed in neurons and to have important functions in neuronal development and/or maintenance of neuronal integrity (see Discussion). The iTRAQ results are in agreement with the increase of hexosaminidase A activity (Fig. 3A) and cathepsin D (Fig. 3C) in lysosomal fractions as well as of palmitoyl-protein thioesterase 1 activity in cathepsin $B^{-/-}/L^{-/-}$ brain lysates [22]. Exemplary tandem mass (MS/MS) spectra of Rab14, calcyon, carboxypeptidase E, and Delta/Notch-like epidermal growth factor-related receptor (DNER) are illustrated in Fig. 5. These proteins were more than 10-fold increased in cathepsin $B^{-/-}/L^{-/-}$ fractions.

3.3. Differential expression of elevated proteins

A hallmark and the first histologically detectable feature of cathepsin $B^{-/-}/L^{-/-}$ mice are dense accumulations of round globules in axon-rich areas such as the corpus callosum (Fig. 1B; Table 1). By electron microscopy, these structures were shown to correspond to expanded axons containing a large number of dense bodies (Fig. 1C, D) [22]. Immunohistological analyses demonstrated that only antibodies against Rab14 and DNER markedly stained these swollen axons (Fig. 6A, B). An

Table 2
Summary of proteins that show more than four-fold increased iTRAQ™ ratios in cathepsin $B^{-/-}/L^{-/-}$ lysosomes (iTRAQ™114: cathepsin $B^{-/-}/L^{-/-}$ lysosomes; iTRAQ™117: wild type)

Accession no.	Protein	Unique peptides	AvG.: 114:117	SD
gi|18390323	Rab14	2	14.4	3.1
gi|31543351	Neuron specific gene family member 1/ Calcyon	3	11.6	2.6
gi|22203763	Carboxypeptidase E	8	10.7	2.3
gi|23097346	Delta/notch-like EGF-related receptor	1	10.2	2.6
gi|26348058	KIAA1414	2	9.9	2.5
gi|31560090	Unnamed protein product: Laminin A domain	4	7.7	2.4
gi|33440473	Protein phosphatase 2 (formerly 2A), regulatory subunit A (PR 65), beta isoform	4	7.5	1.1
gi|34328185	Prosaposin	7	6.9	1.8
gi|38080221	similar to Elongation factor 1-alpha 1 (EF-1-alpha-1)	3	6.9	1.0
gi|28972311	Neurochondrin	2	5.7	0.6
gi|6679451	Palmitoyl-protein thioesterase 1	6	5.4	1.0
gi|6753102	Apolipoprotein E precursor (Apo-E)	5	5.4	1.0
gi|6753556	Cathepsin D	10	5.2	1.1
gi|6754186	Hexosaminidase B	10	4.7	1.2
gi|6754954	Sequestosome 1, oxidative stress induced	3	4.6	0.6
gi|7110627	Hexosaminidase A	2	4.5	0.7
gi|6755919	Ubiquitin B	5	4.3	1.2
gi|21735433	N-acylsphingosine amidohydrolase (acid ceramidase)-like; Asahl protein	4	4.3	1.1
gi|7242181	Phospholipase D3	7	4.3	1.2

Increased hemoglobins are not listed since it seems likely that intracardiac perfusion of the cachectic double mutant mice was inefficient. Exploratory experiments had shown that hemoglobins contaminate late-stage lysosomal fractions: A red band was visible in wildtype and cathepsin $B^{-/-}/L^{-/-}$ Percoll gradients which disappeared upon perfusion (data not shown).

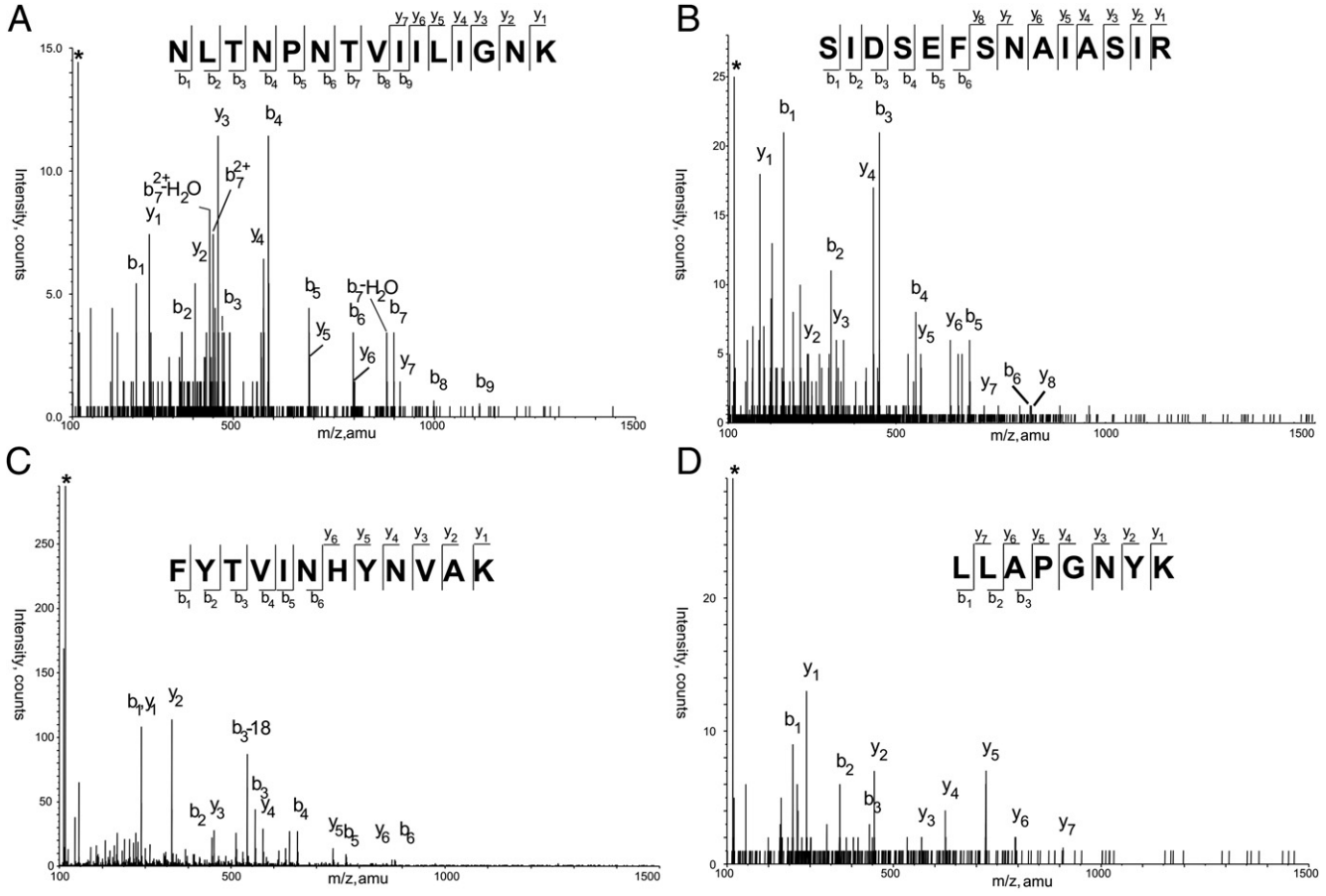

Fig. 5. Exemplary peptide MS/MS spectra of Rab14 (A), DNER (B), calcyon (C), and carboxypeptidase E (D) using iTRAQ™. Respective peptide sequences are given in the spectra. Asterisks indicate the iTRAQ™114 fragment ions derived from cathepsin $B^{-/-}/L^{-/-}$ lysosomes. The wild type lysosomes are labeled with iTRAQ™117. In each case the iTRAQ™114 fragment ion shows substantially higher intensities than the respective iTRAQ™117 signal. The signals related to the b- and y-ion series are annotated in both the spectra and the corresponding peptide sequence.

antibody against cathepsin D labeled perikarya of many cell types throughout the cerebral grey and white matter, but not the pathologically swollen axons in cathepsin $B^{-/-}/L^{-/-}$ mice (Fig. 6C). Cathepsin D staining of perikarya was more pronounced in cathepsin $B^{-/-}/L^{-/-}$ brains (data not shown). Rab14 and DNER were also increased in perikarya of select $B^{-/-}/L^{-/-}$ cortical neurons (data not shown). Thus, immunohistological analyses of Rab14 and DNER for whom functional antibodies were available do not only show a gradual quantitative, but a qualitative difference.

4. Discussion

The proteomics-approach involving relative quantification of protein abundance has led to the identification of 19 different proteins with significantly increased abundance levels in cathepsin $B^{-/-}/L^{-/-}$ cerebral lysosomes. Comparable strategies have recently been employed successfully for similar analyses directed towards e.g. lysosomal membranes or neuromelanine granules [32,36,37]. Although such a proteomics-approach cannot guarantee completeness of the obtained dataset, it has added valuable information for deeper insight into lysosomal function. Notably, the current study focused on the analysis of accumulating neuron-specific proteins in lysosomal storage bodies of murine brains deficient in the two proteases cathepsin B and L. Decreased proteins were not further analyzed since the reduction of any protein in double-deficient brains would rather reflect a general disturbance of metabolism by the advanced pathological process than a specific downregulation.

The largest group of proteins that were increased at least four-fold in cathepsin $B^{-/-}/L^{-/-}$ cerebral lysosomes were lysosomal enzymes as well as molecules associated with the ubiquitin-conjugating system. Elevated levels of lysosomal enzymes have been found in other diseases with impaired lysosomal function such as the neuronal ceroid lipofuscinoses. This has been interpreted as a compensatory mechanism [38] which is supported by the observation that palmitoyl-protein thioesterase 1 and tripeptidyl-peptidase 1 activities were normal in 12-day-old and elevated only in older cathepsin $B^{-/-}/L^{-/-}$ brain lysates in response to disease progression (Table 1) [22]. Ubiquitin-positive inclusion bodies are also common findings in neurodegenerative diseases including lysosomal storage disorders [39]. Therefore, increased levels of lysosomal and ubiquitin-associated proteins presumably are not a major disease-causing mechanism in cathepsin $B^{-/-}/L^{-/-}$ mice.

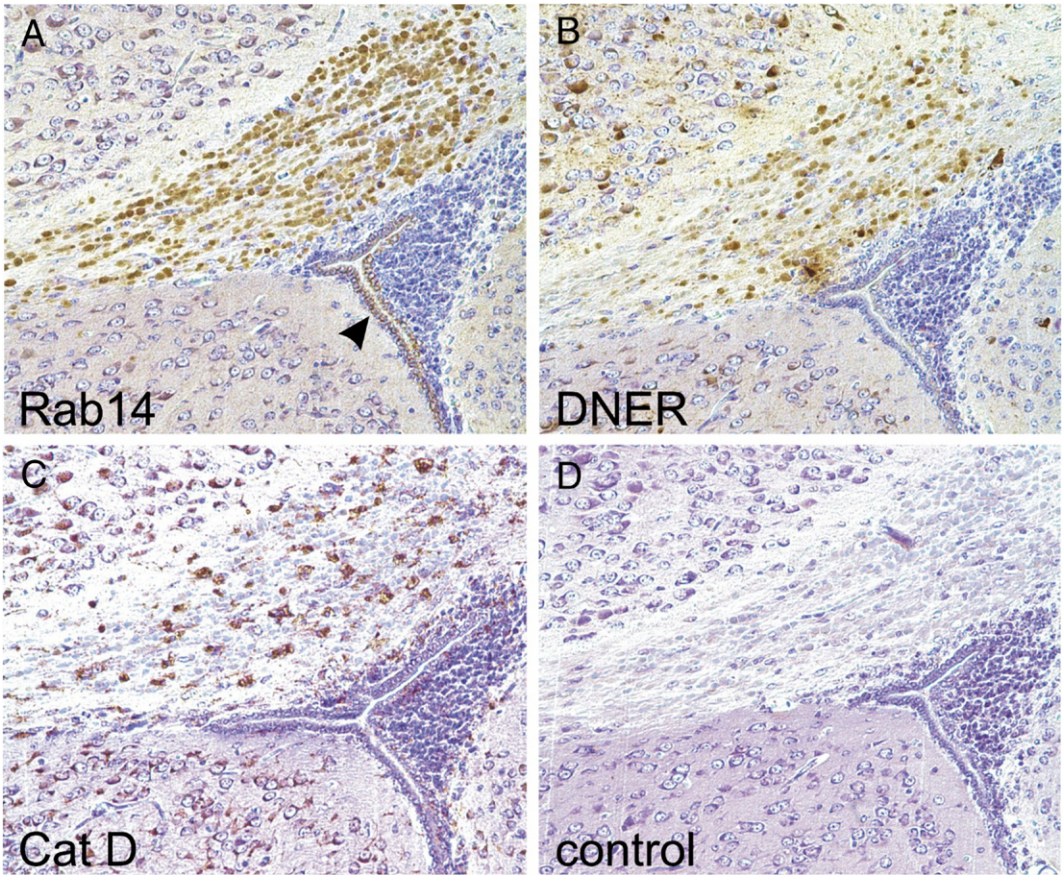

Fig. 6. Densely packed, expanded axons in axon-rich areas of cathepsin $B^{-/-}/L^{-/-}$ brains such as the corpus callosum are Rab14- and DNER-positive (A, B, brown round globules). Note that Rab14 also stains ependymal cells lining the ventricle (arrow head). (C) Immunohistochemistry with an antibody against cathepsin D (Cat D) fails to stain the swollen axons while cell somata of various cell types throughout the brain are cathepsin D-positive (brown). (D) A control $B^{-/-}/L^{-/-}$ section without first antibody shows blue round globules stained with cresylecht violet.

Neurons in the central nervous system can synthesize apolipoprotein E in response to stress or injury (reviewed in [40]). Apolipoprotein E is a prototypic secretory and endocytosed protein which has also been colocalized with CD63- and cathepsin D-positive lysosomes in cultured human brain neurons [31]. Apolipoprotein E plays important roles in maintenance and repair of neurons including stimulation of neurite outgrowth and synaptic plasticity. Therefore, the expression of apolipoprotein E by cathepsin $B^{-/-}/L^{-/-}$ neurons, astrocytes or activated microglia may be induced to promote neuron protection.

Another protein which is six-fold increased in cathepsin $B^{-/-}/L^{-/-}$ lysosomes is neurochondrin. Neurochondrin has been reported to be prominently expressed in zones of neurite outgrowth and to bind to the cytoplasmic domain of the synaptic transmembrane-type semaphorin4C [41–43]. Neurochondrin also binds to phosphatic acid [44] which is produced by phospholipase D1 and has been implicated in vesicular trafficking and phagocytosis [45]. The phospholipase D3 isoform is elevated in cathepsin $B^{-/-}/L^{-/-}$ cerebral lysosomes. While phospholipase D1 plays an important role in neurotransmitter release [46], phospholipase D3 is thus far not intensively characterized but known to be expressed in the murine telencephalon during postnatal development [47].

Rab14, carboxypeptidase E, calcyon, and the Delta/Notch-like epidermal growth factor-related receptor (DNER) are the most prominently increased proteins in cathepsin $B^{-/-}/L^{-/-}$ cerebral lysosomal fractions when compared to the corresponding wildtype fractions (Table 2). Rab14 [48] and carboxypeptidase E [34] are two proteins with predominant expression in brain and roles in neuropeptide biosynthesis, secretion, and recycling. Rab 14 is a member of the novel Rab2/4/14 subgroup which is thought to be involved in membrane trafficking between early endosomes and the Golgi cisternae [49]. Rab 4 regulates the recycling of receptors from early endosomes to recycling endosomes and the cell surface and is thus suggested to function at the level of the early sorting endosome [50]. The exact role for Rab14 remains unknown. GFP-Rab14 vesicles co-localized with early endosomal AP1 clathrin-coated vesicles but not with Rab 7 late endosomal vesicles or Lamp2- and Lysotracker-positive lysosomes [49]. A hallmark of the cathepsin $B^{-/-}/L^{-/-}$ phenotype are densely packed axonal inclusions [22] (Fig. 1B; Table 1). Expanded axons specifically reacted with antibodies against Rab14 and DNER but not with an antibody against the lysosomal marker cathepsin D (Fig. 6). The neuron-specific transmembrane protein DNER is normally expressed in somatodentritic endosomal compartments of the developing central nervous system [35], promotes neuron–glia

interaction by activating Notch signalling [51], and is essential for cerebellar development [52]. Apart from singular cell somata, no DNER-staining was observed within white matter of wild type mice in agreement with the previously reported somatodendritic expression of DNER (data not shown). Only expanded axons of double mutant mice were DNER-positive. It could therefore be possible that Rab-14 and DNER-positive, but cathepsin D-negative endosomal compartments evade towards axons in cathepsin $B^{-/-}/L^{-/-}$ neurons which are overloaded with lysosomes due to defective protein turnover. The increase of Rab14-positive dense bodies could be a compensatory rescue mechanism to relieve the lysosomal compartment via release of vesicle content. While unique in location and dense packing in cathepsin $B^{-/-}/L^{-/-}$ mice, phenotypically similar axonal inclusions have been observed in human lysosomal diseases [53]. The role of Rab14 and DNER in these disorders remains to be shown.

Intriguingly, the occurrence of axonal swellings precedes lysosomal storage in neuronal perikarya [22] (Fig. 1B; Table 1). Cathepsin $B^{-/-}/L^{-/-}$ mice develop this neuronal phenotype during early postnatal development, a phase characterized by intensive synaptogenesis as well as extensive growth and degeneration [54]. It is therefore also conceivable that sorting/recycling of Rab14- and DNER-positive endosomal compartments could be impaired in double mutant mice. This would suggest two different disease-causing mechanisms for cathepsin $B^{-/-}/L^{-/-}$ neurodegeneration: lysosomal storage due to defective terminal degradation of proteins and (a) more specific pathomechanism(s). Thus far, nothing is known about calcyon expression and function in early postnatal development of the murine brain. Calcyon is a 24-kDa transmembrane protein predominantly expressed in brain and localized to vesicular compartments in neuronal cell bodies, dendrites, spines, and synaptic structures. Initially, calcyon was found to interact with the D1 dopamine receptor in pyramidal cells of the prefrontal cortex [55]. Later, the clathrin light chain was identified as a further interaction partner of calcyon which was found to be a stimulator of clathrin-mediated endocytosis in cortical neurons [29]. With our current approach, we have only analyzed the lysosomal compartment. It will be interesting to analyze whether cathepsins B and L influence calcyon-mediated synaptic plasticity, vesicle recycling or transport in postnatal neuronal development. The specific roles of Rab14, DNER, calcyon, and carboxypeptidase E in the secretory or endosomal compartments during early postnatal development of the central nervous system could be directly or indirectly regulated by degradation or processing through cathepsins B and L. Defective neuropeptide production, secretion, vesicle sorting or recycling could contribute to the accumulation of lysosomal and misrouting of endosomal compartments in cathepsin $B^{-/-}/L^{-/-}$ neurons.

Acknowledgements

We thank C. Peters for providing cathepsin $B^{-/-}$ mice, AstraZeneca for cathepsin $L^{-/-}$ mice, and S. Gätzner for expert technical assistance. This work was supported by the Graduierten-kolleg 1048 and an Emmy Noether-grant from the Deutsche Forschungsgemeinschaft (Fe 432/6-5).

References

[1] B. Goulet, A. Baruch, N.S. Moon, M. Poirier, L.L. Sansregret, A. Erickson, M. Bogyo, A. Nepveu, A cathepsin L isoform that is devoid of a signal peptide localizes to the nucleus in S phase and processes the CDP/Cux transcription factor, Mol. Cell 14 (2004) 207–219.
[2] T. Nakagawa, W. Roth, P. Wong, A. Nelson, A. Farr, J. Deussing, J.A. Villadangos, H. Ploegh, C. Peters, A.Y. Rudensky, Cathepsin L: critical role in Ii degradation and CD4 T cell selection in the thymus, Science 280 (1998) 450–453.
[3] T. Reinheckel, S. Hagemann, S. Dollwet-Mack, E. Martinez, T. Lohmuller, G. Zlatkovic, D.J. Tobin, N. Maas-Szabowski, C. Peters, The lysosomal cysteine protease cathepsin L regulates keratinocyte proliferation by control of growth factor recycling, J. Cell Sci. 118 (2005) 3387–3395.
[4] B. Friedrichs, C. Tepel, T. Reinheckel, J. Deussing, K. von Figura, V. Herzog, C. Peters, P. Saftig, K. Brix, Thyroid functions of mouse cathepsins B, K, and L, J. Clin. Invest. 111 (2003) 1733–1745.
[5] S. Yasothornsrikul, D. Greenbaum, K.F. Medzihradszky, T. Toneff, R. Bundey, R. Miller, B. Schilling, I. Petermann, J. Dehnert, A. Logvinova, P. Goldsmith, J.M. Neveu, W.S. Lane, B. Gibson, T. Reinheckel, C. Peters, M. Bogyo, V. Hook, Cathepsin L in secretory vesicles functions as a prohormone-processing enzyme for production of the enkephalin peptide neurotransmitter, Proc. Natl. Acad. Sci. U. S. A. 100 (2003) 9590–9595.
[6] V. Hook, S. Yasothornsrikul, D. Greenbaum, K.F. Medzihradszky, K. Troutner, T. Toneff, R. Bundey, A. Logrinova, T. Reinheckel, C. Peters, M. Bogyo, Cathepsin L and Arg/Lys aminopeptidase: a distinct prohormone processing pathway for the biosynthesis of peptide neurotransmitters and hormones, Biol. Chem. 385 (2004) 473–480.
[7] V.Y. Hook, Protease pathways in peptide neurotransmission and neurodegenerative diseases, Cell. Mol. Neurobiol. 26 (2006) 449–469.
[8] S. Mueller-Steiner, Y. Zhou, H. Arai, E.D. Roberson, B. Sun, J. Chen, X. Wang, G. Yu, L. Esposito, L. Mucke, L. Gan, Antiamyloidogenic and neuroprotective functions of cathepsin B: implications for Alzheimer's disease, Neuron 51 (2006) 703–714.
[9] F. Authier, M. Metioui, A.W. Bell, J.S. Mort, Negative regulation of epidermal growth factor signaling by selective proteolytic mechanisms in the endosome mediated by cathepsin B, J. Biol. Chem. 274 (1999) 33723–33731.
[10] F. Authier, M. Kouach, G. Briand, Endosomal proteolysis of insulin-like growth factor-I at its C-terminal D-domain by cathepsin B, FEBS Lett. 579 (2005) 4309–4316.
[11] K. Chandran, N.J. Sullivan, U. Felbor, S.P. Whelan, J.M. Cunningham, Endosomal proteolysis of the Ebola virus glycoprotein is necessary for infection, Science 308 (2005) 1643–1645.
[12] G. Simmons, D.N. Gosalia, A.J. Rennekamp, J.D. Reeves, S.L. Diamond, P. Bates, Inhibitors of cathepsin L prevent severe acute respiratory syndrome coronavirus entry, Proc. Natl. Acad. Sci. U. S. A. 102 (2005) 11876–11881.
[13] U. Felbor, L. Dreier, R.A. Bryant, H.L. Ploegh, B.R. Olsen, W. Mothes, Secreted cathepsin L generates endostatin from collagen XVIII, EMBO J. 19 (2000) 1187–1194.
[14] V. Gocheva, W. Zeng, D. Ke, D. Klimstra, T. Reinheckel, C. Peters, D. Hanahan, J.A. Joyce, Distinct roles for cysteine cathepsin genes in multistage tumorigenesis, Genes Dev. 20 (2006) 543–556.
[15] L. Foghsgaard, D. Wissing, D. Mauch, U. Lademann, L. Bastholm, M. Boes, F. Elling, M. Leist, M. Jaattela, Cathepsin B acts as a dominant execution protease in tumor cell apoptosis induced by tumor necrosis factor, J. Cell Biol. 153 (2001) 999–1010.
[16] G. Kroemer, M. Jaattela, Lysosomes and autophagy in cell death control, Nat. Rev., Cancer 5 (2005) 886–897.
[17] N. Liu, S.M. Raja, F. Zazzeroni, S.S. Metkar, R. Shah, M. Zhang, Y. Wang, D. Bromme, W.A. Russin, J.C. Lee, M.E. Peter, C.J. Froelich, G. Franzoso, P.G. Ashton-Rickardt, NF-kappaB protects from the lysosomal pathway of cell death, EMBO J. 22 (2003) 5313–5322.

[18] M.K. Houseweart, L.A. Pennacchio, A. Vilaythong, C. Peters, J.L. Noebels, R.M. Myers, Cathepsin B but not cathepsins L or S contributes to the pathogenesis of Unverricht–Lundborg progressive myoclonus epilepsy (EPM1), J. Neurobiol. 56 (2003) 315–327.
[19] V. Stoka, B. Turk, S.L. Schendel, T.H. Kim, T. Cirman, S.J. Snipas, L.M. Ellerby, D. Bredesen, H. Freeze, M. Abrahamson, D. Bromme, S. Krajewski, J.C. Reed, X.M. Yin, V. Turk, G.S. Salvesen, Lysosomal protease pathways to apoptosis. Cleavage of bid, not pro-caspases, is the most likely route, J. Biol. Chem. 276 (2001) 3149–3157.
[20] M.K. Houseweart, A. Vilaythong, X.M. Yin, B. Turk, J.L. Noebels, R.M. Myers, Apoptosis caused by cathepsins does not require Bid signaling in an in vivo model of progressive myoclonus epilepsy (EPM1), Cell Death Differ. 10 (2003) 1329–1335.
[21] A. Wille, A. Gerber, A. Heimburg, A. Reisenauer, C. Peters, P. Saftig, T. Reinheckel, T. Welte, F. Buhling, Cathepsin L is involved in cathepsin D processing and regulation of apoptosis in A549 human lung epithelial cells, Biol. Chem. 385 (2004) 665–670.
[22] U. Felbor, B. Kessler, W. Mothes, H.H. Goebel, H.L. Ploegh, R.T. Bronson, B.R. Olsen, Neuronal loss and brain atrophy in mice lacking cathepsins B and L, Proc. Natl. Acad. Sci. U. S. A. 99 (2002) 7883–7888.
[23] M. Koike, M. Shibata, S. Waguri, K. Yoshimura, I. Tanida, E. Kominami, T. Gotow, C. Peters, K. von Figura, N. Mizushima, P. Saftig, Y. Uchiyama, Participation of autophagy in storage of lysosomes in neurons from mouse models of neuronal ceroid-lipofuscinoses (Batten disease), Am. J. Pathol. 167 (2005) 1713–1728.
[24] M. Koike, H. Nakanishi, P. Saftig, J. Ezaki, K. Isahara, Y. Ohsawa, W. Schulz-Schaeffer, T. Watanabe, S. Waguri, S. Kametaka, M. Shibata, K. Yamamoto, E. Kominami, C. Peters, K. von Figura, Y. Uchiyama, Cathepsin D deficiency induces lysosomal storage with ceroid lipofuscin in mouse CNS neurons, J. Neurosci. 20 (2000) 6898–6906.
[25] J. Tyynela, I. Sohar, D.E. Sleat, R.M. Gin, R.J. Donnelly, M. Baumann, M. Haltia, P. Lobel, A mutation in the ovine cathepsin D gene causes a congenital lysosomal storage disease with profound neurodegeneration, EMBO J. 19 (2000) 2786–2792.
[26] R. Steinfeld, K. Reinhardt, K. Schreiber, M. Hillebrand, R. Kraetzner, W. Bruck, P. Saftig, J. Gartner, Cathepsin D deficiency is associated with a human neurodegenerative disorder, Am. J. Hum. Genet. 78 (2006) 988–998.
[27] E. Siintola, S. Partanen, P. Stromme, A. Haapanen, M. Haltia, J. Maehlen, A.E. Lehesjoki, J. Tyynela, Cathepsin D deficiency underlies congenital human neuronal ceroid-lipofuscinosis, Brain 129 (2006) 1438–1445.
[28] Y. Wagner, A. Sickmann, H.E. Meyer, G. Daum, Multidimensional nano-HPLC for analysis of protein complexes, J. Am. Soc. Mass Spectrom. 14 (2003) 1003–1011.
[29] J. Xiao, R. Dai, L. Negyessy, C. Bergson, Calcyon, a novel partner of clathrin light chain, stimulates clathrin-mediated endocytosis, J. Biol. Chem. 281 (2006) 15182–15193.
[30] R.M. Dekroon, P.J. Armati, Synthesis and processing of apolipoprotein E in human brain cultures, Glia 33 (2001) 298–305.
[31] R.M. DeKroon, P.J. Armati, The endosomal trafficking of apolipoprotein E3 and E4 in cultured human brain neurons and astrocytes, Neurobiol. Dis. 8 (2001) 78–89.
[32] R.D. Bagshaw, D.J. Mahuran, J.W. Callahan, Lysosomal membrane proteomics and biogenesis of lysosomes, Mol. Neurobiol. 32 (2005) 27–41.
[33] G.M. Jenkins, M.A. Frohman, Phospholipase D: a lipid centric review, Cell. Mol. Life Sci. 62 (2005) 2305–2316.
[34] D.R. Cool, E. Normant, F. Shen, H.C. Chen, L. Pannell, Y. Zhang, Y.P. Loh, Carboxypeptidase E is a regulated secretory pathway sorting receptor: genetic obliteration leads to endocrine disorders in Cpe(fat) mice, Cell 88 (1997) 73–83.
[35] M. Eiraku, Y. Hirata, H. Takeshima, T. Hirano, M. Kengaku, Delta/notch-like epidermal growth factor (EGF)-related receptor, a novel EGF-like repeat-containing protein targeted to dendrites of developing and adult central nervous system neurons, J. Biol. Chem. 277 (2002) 25400–25407.
[36] J. Hu, J. Qian, O. Borisov, S. Pan, Y. Li, T. Liu, L. Deng, K. Wannemacher, M. Kurnellas, C. Patterson, S. Elkabes, H. Li, Optimized proteomic analysis of a mouse model of cerebellar dysfunction using amine-specific isobaric tags, Proteomics (2006).
[37] F. Tribl, M. Gerlach, K. Marcus, E. Asan, T. Tatschner, T. Arzberger, H.E. Meyer, G. Bringmann, P. Riederer, "Subcellular proteomics" of neuromelanin granules isolated from the human brain, Mol. Cell Proteomics 4 (2005) 945–957.
[38] J. Ezaki, E. Kominami, The intracellular location and function of proteins of neuronal ceroid lipofuscinoses, Brain Pathol. 14 (2004) 77–85.
[39] S.S. Zhan, K. Beyreuther, H.P. Schmitt, Neuronal ubiquitin and neurofilament expression in different lysosomal storage disorders, Clin. Neuropathol. 11 (1992) 251–255.
[40] R.W. Mahley, K.H. Weisgraber, Y. Huang, Apolipoprotein E4: a causative factor and therapeutic target in neuropathology, including Alzheimer's disease, Proc. Natl. Acad. Sci. U. S. A. 103 (2006) 5644–5651.
[41] R. Istvanffy, D.M. Vogt Weisenhorn, T. Floss, W. Wurst, Expression of neurochondrin in the developing and adult mouse brain, Dev. Genes Evol. 214 (2004) 206–209.
[42] Y. Ohoka, M. Hirotani, H. Sugimoto, S. Fujioka, T. Furuyama, S. Inagaki, Semaphorin 4C, a transmembrane semaphorin, [corrected] associates with a neurite-outgrowth-related protein, SFAP75, Biochem. Biophys. Res. Commun. 280 (2001) 237–243.
[43] K. Shinozaki, H. Kume, H. Kuzume, K. Obata, K. Maruyama, Norbin, a neurite-outgrowth-related protein, is a cytosolic protein localized in the somatodendritic region of neurons and distributed prominently in dendritic outgrowth in Purkinje cells, Brain Res. Mol. Brain Res. 71 (1999) 364–368.
[44] N.T. Ktistakis, C. Delon, M. Manifava, E. Wood, I. Ganley, J.M. Sugars, Phospholipase D1 and potential targets of its hydrolysis product, phosphatidic acid, Biochem. Soc. Trans. 31 (2003) 94–97.
[45] M. Corrotte, S. Chasserot-Golaz, P. Huang, G. Du, N.T. Ktistakis, M.A. Frohman, N. Vitale, M.F. Bader, N.J. Grant, Dynamics and function of phospholipase D and phosphatidic acid during phagocytosis, Traffic 7 (2006) 365–377.
[46] N. Vitale, A.S. Caumont, S. Chasserot-Golaz, G. Du, S. Wu, V.A. Sciorra, A.J. Morris, M.A. Frohman, M.F. Bader, Phospholipase D1: a key factor for the exocytotic machinery in neuroendocrine cells, EMBO J. 20 (2001) 2424–2434.
[47] K.M. Pedersen, B. Finsen, J.E. Celis, N.A. Jensen, Expression of a novel murine phospholipase D homolog coincides with late neuronal development in the forebrain, J. Biol. Chem. 273 (1998) 31494–31504.
[48] J.R. Junutula, A.M. De Maziere, A.A. Peden, K.E. Ervin, R.J. Advani, S.M. van Dijk, J. Klumperman, R.H. Scheller, Rab14 is involved in membrane trafficking between the Golgi complex and endosome, Mol. Biol. Cell 15 (2004) 2218–2229.
[49] T. Proikas-Cezanne, A. Gaugel, T. Frickey, A. Nordheim, Rab14 is part of the early endosomal clathrin-coated TGN microdomain, FEBS Lett. 580 (2006) 5241–5246.
[50] P. van der Sluijs, M. Hull, P. Webster, P. Male, B. Goud, I. Mellman, The small GTP-binding protein rab4 controls an early sorting event on the endocytic pathway, Cell 70 (1992) 729–740.
[51] M. Eiraku, A. Tohgo, K. Ono, M. Kaneko, K. Fujishima, T. Hirano, M. Kengaku, DNER acts as a neuron-specific Notch ligand during Bergmann glial development, Nat. Neurosci. 8 (2005) 873–880.
[52] A. Tohgo, M. Eiraku, T. Miyazaki, E. Miura, S.Y. Kawaguchi, M. Nishi, M. Watanabe, T. Hirano, M. Kengaku, H. Takeshima, Impaired cerebellar functions in mutant mice lacking DNER, Mol. Cell. Neurosci. 31 (2006) 326–333.
[53] S. Walter, H.H. Goebel, Ultrastructural pathology of dermal axons and Schwann cells in lysosomal diseases, Acta Neuropathol. (Berl.) 76 (1988) 489–495.
[54] N. Aggelopoulos, J.G. Parnavelas, S. Edmunds, Synaptogenesis in the dorsal lateral geniculate nucleus of the rat, Anat. Embryol. (Berl.) 180 (1989) 243–257.
[55] N. Lezcano, L. Mrzljak, S. Eubanks, R. Levenson, P. Goldman-Rakic, C. Bergson, Dual signaling regulated by calcyon, a D1 dopamine receptor interacting protein, Science 287 (2000) 1660–1664.